Adsorption of CO_2 on Amine-Modified Silica Particles in a Confined-Fluidized Bed

Rossella Girimonte [1],* [ID]**, Flaviano Testa [1], Marta Gallo [2]** [ID]**, Rocco Buscieti [1], Giuseppe Leone [1] and Brunello Formisani [1]**

[1] Dipartimento di Ingegneria Informatica, Modellistica, Elettronica e Sistemistica—DIMES, Università della Calabria, 87036 Rende (Cosenza), Italy; flaviano.testa@unical.it (F.T.); rocco_b_90@hotmail.it (R.B.); peppis_1@hotmail.it (G.L.); brunello.formisani@unical.it (B.F.)

[2] Dipartimento di Scienza Applicata e Tecnologia, Politecnico di Torino, 10129 Torino, Italy; marta.gallo@polito.it

* Correspondence: rossella.girimonte@unical.it; Tel.: +39-0984-496689

Abstract: To reduce the anthropogenic CO_2 emissions produced from fossil fuel burning plants, the application of carbon capture and storage (CCS) is necessary and development of a more efficient and economically feasible CO_2 capture process is essential as an alternative to the conventional amine scrubbing process which uses aqueous amine solutions. CO_2 capture can be enhanced by improving both the gas–solid contact efficiency and by tuning a specific high-performance sorbent. The aim of this research is to investigate the adsorption of CO_2 using impregnated mesoporous silica in a "confined-fluidized bed". This non-conventional fluidized bed (sometimes also termed the "packed-fluidized bed") seems suitable for improving the efficiency of gas–solid processes for which the bypass effect of the gas–solid contact caused by bubbling represents a major drawback. Results, expressed as grams of CO_2 adsorbed per kilogram of material, are discussed in terms of amine load in the sorbent, breakthrough time and fraction of bed utilized. The stability of the materials after regeneration cycles is also discussed. The results obtained confirm that the confinement of the bed allows exploiting fluidization technology in adsorption operations. The operating velocity can be fixed at a value at which the thermal effects also connected to the operation are kept under control.

Keywords: CO_2 capture; adsorption; amine-based adsorbents; mesoporous silica gel; packed-fluidized bed; confined-fluidized bed

1. Introduction

The estimates released in a new report from the Global Carbon Project, an international research consortium dedicated to tracking the world's greenhouse gas emissions, represents an increasing long-term trend of the total carbon emissions from all human activities, including industrial activities and burning of fossil fuels, agriculture and land use [1]. International climate goals outlined in the Paris Agreement will be harder to reach as long as burning coal will be the cheapest way of generating energy and coal is relatively abundant in large energy-consuming countries. So far, Carbon dioxide Capture and Storage (CCS) is considered the most promising post-combustion technology to sequestrate CO_2 from large stationary sources of CO_2 emissions [2].

The presence of other contaminants in the exhaust gas, such as NO_x, SO_x, and particulate matter, are not crucial because they are usually separated before the CO_2 capture process, but the low partial pressure of CO_2 in the flue gas at atmospheric pressure, derived by the CO_2 concentration within 13–15%, is the limiting factor, as it is a very low driving force for its separation. For this reason, monoethanolamine-based chemical absorption or a scrubbing process is currently the most suitable

technology to be implemented. However, although chemical absorption technology is more mature, its character of being energy intensive is still motivating many scientists to find alternatives [3]; in fact, the overall cost of a CO_2 capture process is 52–77 USD/tonnes CO_2 [4] and most energy consumption comes from the solvent regeneration step, occupying about 60% of the required energy. Moreover, other drawbacks are also present: low CO_2 loading capacity, high equipment corrosion rate and large equipment size and amine degradation by SO_2, NO_2 and O_2 in the flue gases which induces a high absorbent makeup rate. Many researchers indicate the solid adsorption process as an alternative to achieve the purpose of CO_2 capture. As described in several reviews on CO_2 capture by adsorption [5,6], an appropriate CO_2 adsorbent should satisfy the following characteristics: (1) low-cost of raw materials, (2) low heat capacity, (3) fast kinetics, (4) high CO_2 adsorption capacity, (5) high CO_2 selectivity and (6) thermal, chemical and mechanical stability under extensive cycling. In the huge variety of solid adsorbents proposed [7], many studies have been devoted to improving CO_2 adsorption and selectivity by chemical modification of the surface of solid materials possessing a high surface area. Among these, a new tentative study by Quang et al. (2013) [8] proposed using an ordered mesoporous silica as a candidate because of its high surface area, high pore volume, tuneable pore size and good thermal and mechanical stability.

However, the CO_2 adsorption capacity, especially at atmospheric pressure, is not as high as the amount of surface OH groups which are a key factor for improving CO_2 adsorption capacity and selectivity for a flue gas with low CO_2 partial pressure. The interaction between acidic CO_2 molecules and modified basic active sites on the surface facilitates CO_2 adsorption through the formation of covalent bonding. Typically, there are three frequently introduced methods to prepare amine-based adsorbent for CO_2 capture—i.e., (1) impregnating mono or polymer amines on a porous structure, (2) grafting amino functional groups onto a substrate by a functionalization method and (3) coprecipitation of amine compounds with silica during synthesis.

Previous studies on fluidization in a "confined-fluidized bed", sometimes also termed "packed-fluidized bed" [9–12], have confirmed this non-conventional fluidization technology as a valuable way to suppress bubble flow in a fluidized regime for solids belonging to Class B of Geldart's classification. The interstice network provided by a packed coarse solid (i.e., not subjected to suspension by the gas at any velocity) constitutes the confining environment in which the sorbent, much finer than the packed solid, can first achieve the fluidized state and then homogeneously expand without the formation of gas bubbles, as they have no room to form. As a consequence, in systems of this type the efficiency of gas–solid processes for which the bypass effect associated with bubbling is a major drawback showed improved results. Among these, CO_2 capture can be enhanced by improving the gas–solid contact efficiency [13,14].

The aim of this research is to investigate the adsorption of CO_2 using an impregnated mesoporous silica in a confined-fluidized bed. A detailed analysis is provided to describe the effect of amination pre-treatment concerning the enhancement of adsorption of CO_2 and in terms of the effect of the operating velocity on the performance of a confined-fluidized bed of amine-modified silica particles. The stability of the materials after regeneration cycles is also discussed.

2. Materials and Methods

2.1. Experimental Apparatus

The experimental campaign concerning tests of CO_2 adsorption was carried out in a laboratory-scale fluidization column made of plexiglas, with an internal diameter of 50 mm and 700 mm high, equipped with a porous plate between the two flanges at its bottom, acting as a gas distributor. The experimental facility is schematized in Figure 1.
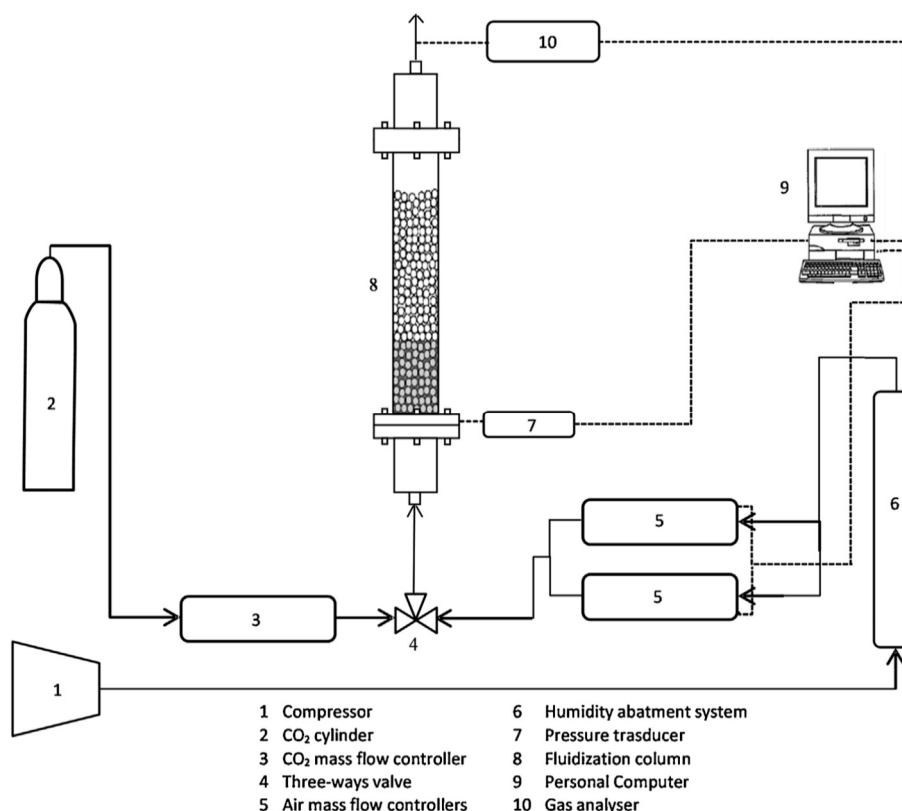
Figure 1. Experimental apparatus.

In this sketch, the shaded zone represents the bed of fine adsorbent fluidized in the voids of the glass beads forming a much taller fixed bed (the clearer zone in the figure).

Glass beads have a diameter of 11 mm and a density of 2.48 g/cm^3. Their packing, never subjected to fluidization, was always 450 mm high, so that its mass was of 1230 g. In it, a smaller amount of fine adsorbent was loaded by percolating through the voids of the glass beads, this material formed a bed of height H_{fc}, which gradually increases during the fluidization test. The gas utilized for fluidization of the fine adsorbent bed was air, whose flow rates were regulated by a set of two mass flow controllers covering the range $0 \div 6000$ Nl/h. For the adsorption tests, the CO_2 concentration in the gas feed stream was set by adding CO_2 from a cylinder to the air supplied by a compressor. A column filled with zeolites and activated carbon was located before the CO_2 mixing point to remove the humidity of the air. The total pressure drop across the solid bed was measured by a U-tube water manometer. The CO_2 concentration in the gas stream entering or leaving the adsorption unit was measured by a gas analyzer, GA-21 plus (Madur Polska Sp. z o.o., Zgierz, Poland) and acquired on a personal computer. A thermocouple vertically immersed in the bed was used to determine its temperature.

2.2. Adsorbent Preparation and Characterization

Commercial silica gel and the chemical (3-Aminopropyl)triethoxysilane (APTES, >98%) were provided by Sigma-Aldrich (St. Louis, MO, USA). Ethanol (analysis grade) was provided by J.T. Baker-Avantor (Radnor, PA, USA). Before the functionalization procedure, the 400–500 μm sample was prepared by sieving to obtain a sample with a short granulometric dispersion and its particle size distribution, reported in Figure 2, was determined by a laser diffractometer, Helos (Sympatec GmbH, Clausthal-Zellerfeld, Germany). Particle shape was characterized thanks to an image analysis system, Qicpic (Sympatec GmbH, Clausthal-Zellerfeld, Germany) and Figure 3 reports some examples of the images obtained. Characteristic parameters of the distribution obtained are reported in Table 1.
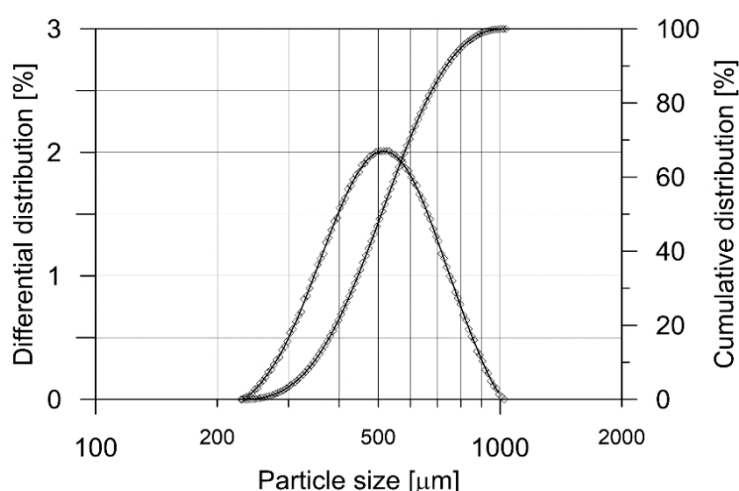
Figure 2. Granulometric distribution curves of the sieved sample of silica gel.

Figure 3. Some images of silica particles (Sympatec-Qicpic).

Table 1. Size and shape properties of the silica particles.

| Sieve Size [μm]	$d_{10\%}$ [μm]	$d_{50\%}$ [μm]	$d_{90\%}$ [μm]	Span [-]	d_v [μm]	φ [-]
400–500	346	509	736	0.768	527	0.75

XRD (X-Ray Diffraction) data were collected using an XPert3 diffractometer (Malvern Panalytical Ltd, Malvern, UK) (Cu Kα radiation λ = 1.5406 Å). Small angles were scanned between 0.7° and 10° 2θ for identifying any possible mesostructure of the material. High angles were scanned between 5° and 60° 2θ in order to verify the presence of order at the atomic scale.

In Figure 4, XRD diffraction at small angles of the silica particles is reported showing the absence of the mesostructure. The XRD diffraction at high angles gives evidence of the amorphous character of the material (figure not reported).

Two functionalized mesoporous silica samples were prepared using a modified procedure reported by Quang et al. (2013) [8]. In total, 100 g of silica gel material was soaked with 400 g of an APTES/ethanol impregnating solution 20/80 (APTES20) and 40/60 (APTES40) w/w in a laboratory flask for 72 h at room temperature and, successively, for 48 h at 40 °C under mechanical stirring. Finally, the slurry was dried in an oven at 60 °C for 48 h. After a CO_2 adsorption test, regeneration cycles were performed heating the powder in an oven at 120 °C for 3 h.

According to the method proposed by Abrahamsen and Geldart (1980) [15], the particle apparent density of the porous adsorbent was determined by comparison with a non-porous solid having the same particle size distribution, similar shape and known density. This method is useful for porous material and is based on the observation that the minimum packed voidage is virtually the same for solids of similar size and particle shape.
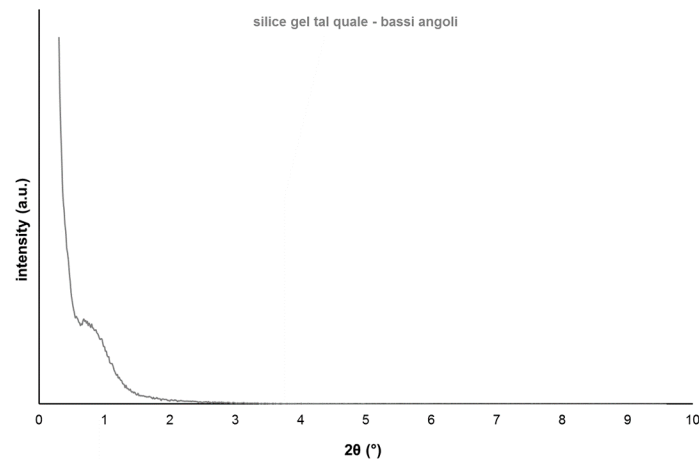
Figure 4. XRD diffraction at small angles for the as-made silica.

In this work, 140 g of a siliceous sand of density ρ = 2.66 g/cm^3, exactly weighed and used as a reference, was loaded into a graduated cylinder and compacted until the minimum volume was reached. A value of voidage of 0.457 was obtained from the relation:

$$\varepsilon = 1 - \frac{\frac{m}{\rho}}{V} \tag{1}$$

Subsequently, the same amount of silica gel was weighed, packed and its occupied volume was determined. Assuming that the voidage of the silica gel particles was equal to that of the reference material when the minimum volume was reached [15]—i.e., that ε_{sand} = $\varepsilon_{mesoporous\text{-}silica}$—application of Equation (1) to silica gel data made it possible to calculate its unknown density, which was equal to 0.947 g/cm^3. The same procedure, applied to two functionalized samples, yielded higher values of particle density, as indicated in Table 2.

Table 2. Particle density, Brunauer–Emmett–Teller (BET) specific surface and Barrett–Joyner–Halenda (BJH) pore volume of the adsorbent particles.

Adsorbent	ρ [kg/m^3]	S_{BET} [m^2/g]	Pore Volume [cm^3/g]
As-made Silica	947	584	0.89
APTES20	1380	180	0.30
APTES40	1520	73	0.10

Nitrogen adsorption-desorption isotherms were acquired using a ASAP 2020 Plus analyzer, (Micromeritics, Norcross, GA, USA). Samples were degassed at 120 °C in nitrogen atmosphere at a pressure of 10 µmHg for 3 h. Surface area was calculated by the Brunauer–Emmett–Teller (BET) method [16] and pore volume by the Barrett–Joyner–Halenda (BJH) method [17] using desorption isothermal data.

Isotherms at 77 K for the three samples studied are reported in Figure 5. The isotherms of as-made silica are of type IV according to the IUPAC (International Union of Pure and Applied Chemistry) classification [18]. Hysteresis loops between 0.5 and 0.9 p/p^0 evidence the presence of mesopores. The surface area calculated with the BET model is 584 m^2/g and the pore volume is 0.89 cm^3/g (see Table 2). These properties make the sample of the as-made silica well suitable for grafting through an impregnation process with APTES.
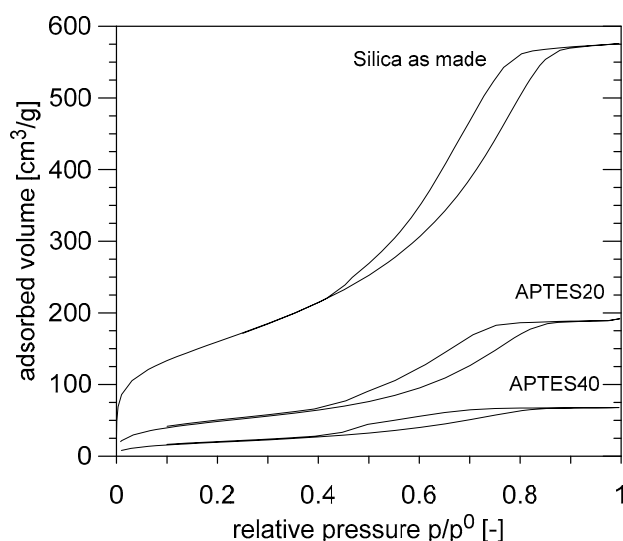
Figure 5. Nitrogen adsorption–desorption isotherms for the as-made silica and two amino-functionalized samples.

In fact, the APTES20 and APTES40 samples adsorbed a considerably lower amount of N_2 with respect to the precursor (S_{BET} of 180 and 73 m^2/g, respectively).

The pore size distribution of the as-made silica (Figure 6) is centred at 5 nm and ranges from 4 to c.a. 13 nm. Pore volume of APTES20 sample is 0.30 cm^3/g and the pore size distribution is similar to that of the as-made material giving evidence that mesopores are not completely occluded. In APTES40, the sample pore volume decreases to 0.10 cm^3/g and only porosity up to 5 nm is present.
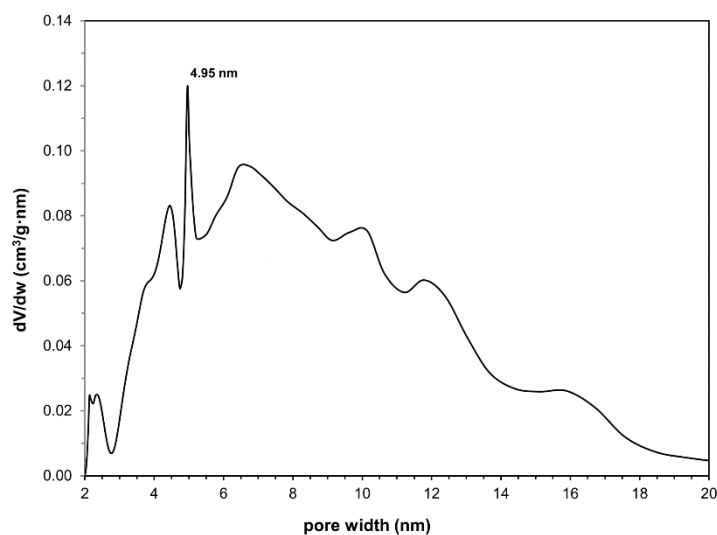
Figure 6. BJH pore size distribution for the as-made silica studied.

Micrographs were obtained using a Field Emission Scanning Electron Microscopy technique by means a Merlin (Zeiss Instruments, Oberkochen, Germany). All the samples were coated with a 5 nm layer of platinum under a tension of 3 kV. In Figure 7, the micrographs of the as-made silica and of APTES20 and APTES40 are compared—the surface of the silica particles is essentially rough but it becomes smooth for the functionalized samples. In addition, small aggregates (up to 200 nm) of the organic molecules are present with a higher population density for the APTES40.

| (**a**) | (**b**) | (**c**) |
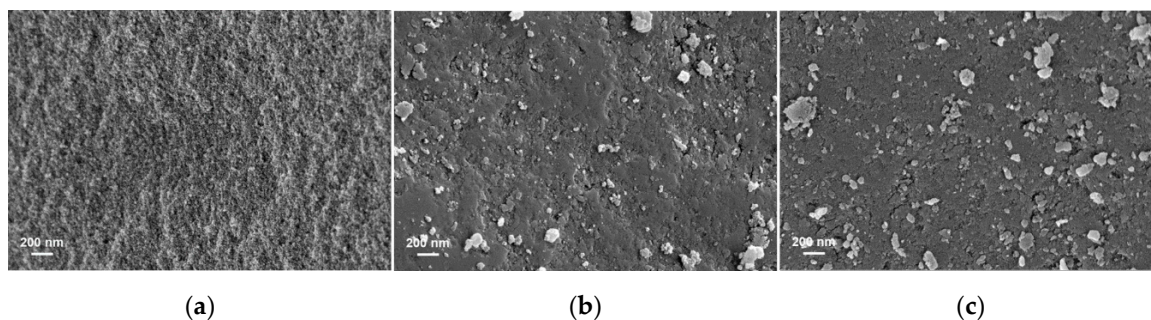
Figure 7. Scanning electron micrographs of: (**a**) as-made silica, (**b**) (3-Aminopropyl)triethoxysilane (APTES)/ethanol impregnating solution 20/80 (APTES20) and (**c**) 40/60 (APTES40).

Thermogravimetric analysis (TGA) was performed using a DSC-TGA STA409C analyzer (Netzsch-Gerätebau GmbH, Selb, Germany) from 20 to 800 °C at a heating rate of 10 °C in static air.

Figure 8 reports the TGA thermograms for the as-made silica, APTES20 and APTES40 samples. Mass loss from room temperature up to ca. 150 °C is attributed to the water physiosorbed on the particles' surfaces. From 120 to 800 °C, vicinal Si-OH groups react with production of H_2O molecules and the formation of -Si-O-Si- groups. When APTES molecules impregnate the silica particles, an important mass loss is present between ca 300 and 600 °C due to degradation and/or combustion of the organic moieties adsorbed or chemically linked on the silica surface. In this case, water is also adsorbed on the organic sites. These data can be utilized for an evaluation of the amount of the APTES molecules. If we consider APTES molecules (MW 221.37 g/moles) as a reference, the amount of the organic moieties is about 55.5 mmol per mol of silica for the APTES20 sample and 89.7 mmol per mol of silica in APTES40.
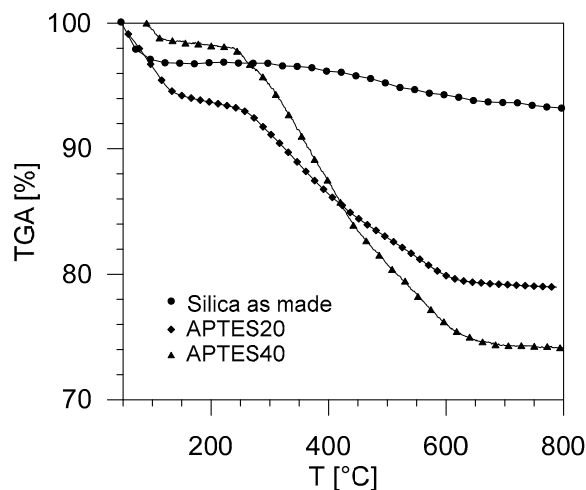
Figure 8. TGA analysis for the as-made silica, APTES20 and APTES40.

2.3. Fluid-Dynamic Characterization

Adsorption tests on the amino-functionalized solids were carried out in a confined-fluidized bed, where the gas–solid contact was verified as being improved [13,14]. In a conventional column, i.e., without packing, the thermal effects of the adsorption process do not recommend a fixed bed configuration for the adsorbent; at the same time, the bubbling regime of the fluidized bed reduces the mass exchange efficiency. These limitations were overcome adopting a non-conventional fluidization technique, by which the fine adsorbent undergoes homogeneous expansion in the voids of the packing of coarse spheres once the state of incipient fluidization is reached. Following the guidelines indicated in a previous study [11], glass beads with a diameter of 11 mm and particle density of 2.48 g/cm^3

were selected as packing particles allowing an interstitial voidage ε_p of 0.44. In a typical experiment of confined fluidization, 1230 g of coarse spheres were poured onto the column. Then, 50 g of the finer solid (the adsorbent) was loaded in the column and, after a complete fluidization–defluidization cycle, their heights were measured (for an aspect ratio H_{fc}/D = 1.6–2.6). The bed voidage in the packed-fluidized bed, i.e., the fraction of volume available to the gas flow, is calculated as:

$$\varepsilon \;=\; 1 - \frac{m_p/\rho_p}{AH_{fc}} - \frac{m_f/\rho_f}{AH_{fc}} \tag{2}$$

where m_p and ρ_p, m_f and ρ_f, are the mass and density of the packing and of the fine sorbent, respectively.

These tests were performed at ambient temperature and pressure. The pressure drop and bed expansion curves obtained by measuring pressure and bed height in experiments performed both at increasing and decreasing superficial gas velocity were found to coincide. Figures 9 and 10 show these diagrams for the three samples investigated—as-made silica and the two solids after functionalization.
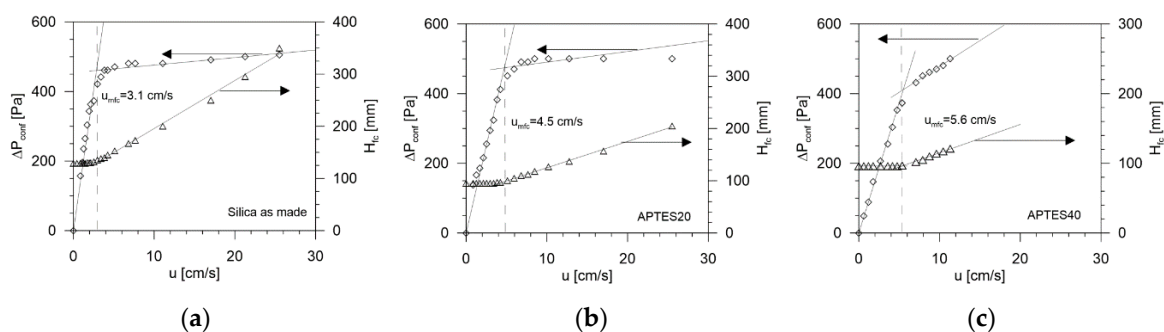
Figure 9. Typical diagram of fluidization tests in a confined bed: pressure drop, ΔP_{conf}, and heigh of the sorbent bed, H_{fc}, versus gas velocity. (**a**) as-made silica; (**b**) APTES20; (**c**) APTES40.
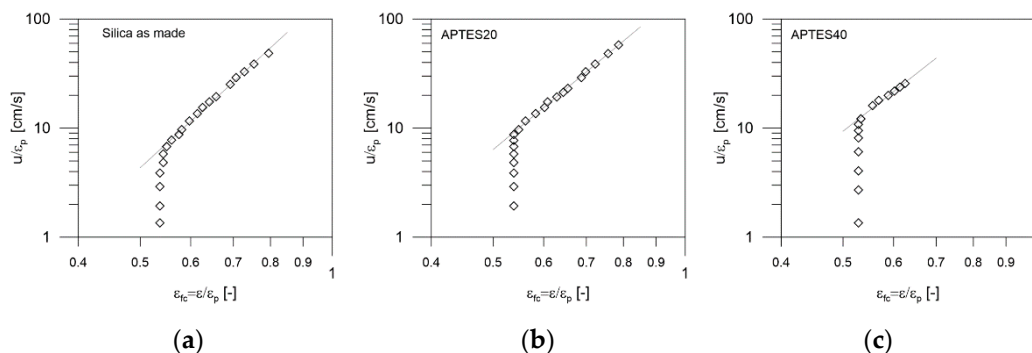
Figure 10. Homogeneous expansion trends for the three samples investigated in a confined bed: (**a**) as-made silica; (**b**) silica APTES20; (**c**) silica APTES40.

As previously shown, the silica gel functionalization changes particle density, a fact that results in a proportional increase in u_{mfc} values (see Figure 9 and data in Table 3).

Table 3. Fluidization properties of the adsorbent particles.

Adsorbent	H_{fc}/D [-]	u_{mfc} [10^{-2} m/s]	ε [-]	$\varepsilon_{fc} = \varepsilon/\varepsilon_p$ [-]	u_0 [10^{-2} m/s]	n [-]
As-made Silica	2.6	3.1	0.236	0.537	189	5.4
APTES20	1.9	4.5	0.237	0.539	187	4.9
APTES40	1.6	5.6	0.233	0.530	204	4.3

On the contrary, the ability of the sorbent to expand in the confined bed configuration remains unchanged. Actually, the homogeneous fluidization parameters ε_{fc}, u_0 and n, as determined from Figure 10, remain almost constant with a little decrease in the exponent n for the sample APTES40, denoting an increased difficulty of expansion through the interstitial voids of the packing (see Table 3).

The regular homogeneous expansion observed was described by a modified form of the Richardson and Zaki's equation [10], in which the exponents n and u_0 are calculated according to a method reported in a previous work [11].

3. Results

3.1. Test on As-Made Silica

The sample of silica gel was tested as a blank potential adsorbent; a test in a conventional fixed bed was carried out with a mixture containing 12.5% of CO_2 and a gas velocity of 3.7 cm/s. A total of 120 g of silica gel was pulled onto the column and, since the minimum fluidization velocity (u_{mf}) is 4.5 cm/s at $\varepsilon_{mf} = 0.43$, the system was in the fixed bed condition, with a constant height equal to 131 mm. The adsorbed mass of CO_2 up to the equilibrium was only 6.15 g/kg of silica, as determined by the breakthrough curve shown in Figure 11. This value is very low and is justified by weak interactions of molecules with a silica surface, characterized only by the presence of silanol groups (SiOH) [8,19,20]. For this reason, a test in the packed-fluidized bed configuration was not carried out, as it was neither useful nor interesting.
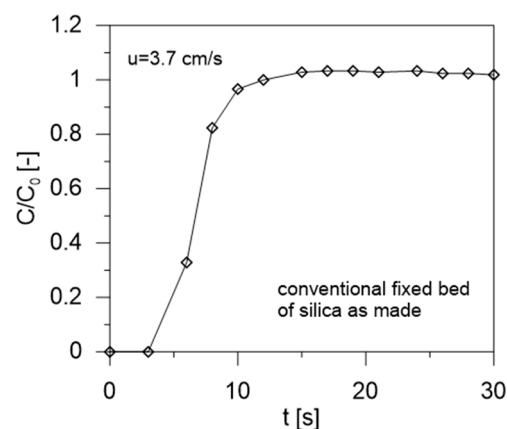

Figure 11. Breakthrough curve for as-made silica in a conventional fixed bed.

3.2. Test on Amino-Functionalized Silica

After functionalization and new dynamic characterization, the solids were used for an adsorption test operated in the confined-fluidized bed configuration. For each sample, two values of the fluidization velocity were chosen in order to analyze the effect of the flow rate on the level of CO_2 capture: 5.7 and 8.6 cm/s for APTES20 and 6.9 and 10.9 cm/s for APTES40. Both values correspond to a condition expansion of the adsorbent over its incipient fluidization velocity threshold. It has to be borne in mind that all the gas fed to the fluidized bed is in contact with the adsorbent; in a packed-fluidized bed the bypass effect in the gas–solid contact typical of the bubbling regime is avoided, so that the value of the gas velocity directly influences the contact time between gas and particles as well as the mass and heat transfer rates. Figures 12–15 show the breakthrough curves (the ratio between the concentration downstream and upstream of the adsorption column versus time) and the temperature trends for both amino-functionalized samples at various values of the superficial velocity of the gas mixture. In order to compare the performance of adsorbents with a different concentration of APTES, a mixture with 12.5% of CO_2 was used in all the adsorption tests and a mass of sorbent of 100 g.
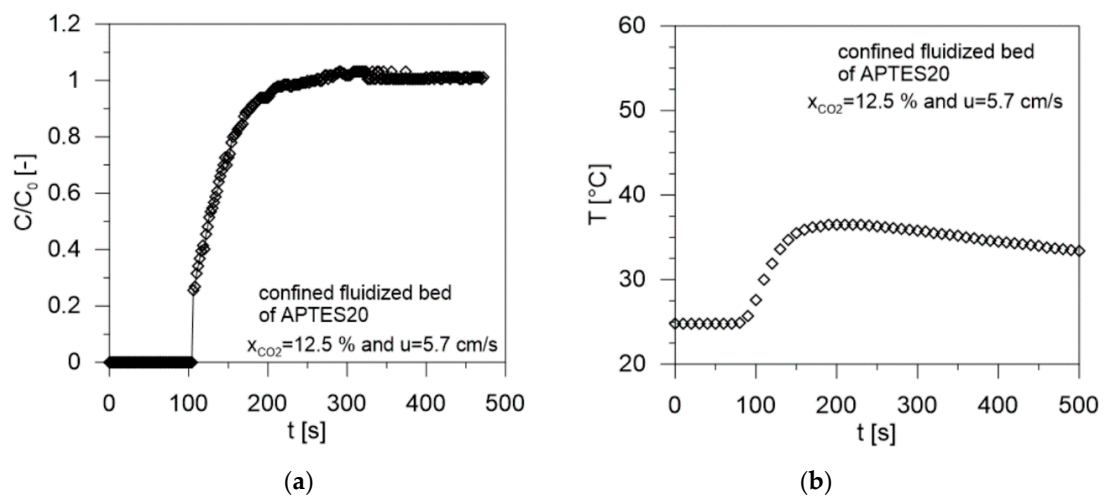
Figure 12. Adsorption test for APTES20 in a confined bed at u = 5.7 cm/s. Mass of adsorbent: 100 g. (**a**) Breakthrough curve; (**b**) temperature trend.
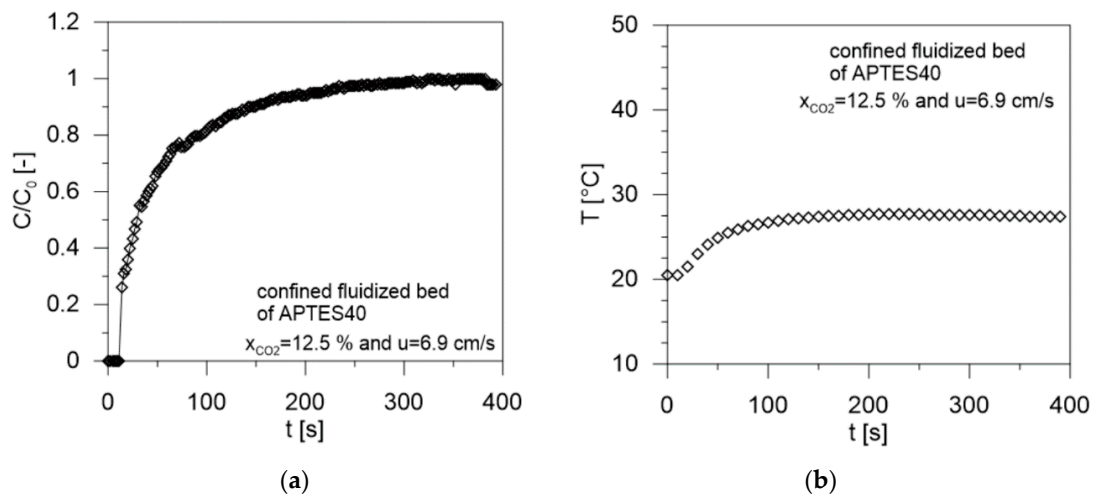
Figure 13. Adsorption test for APTES40 in a confined bed at u = 6.9 cm/s. Mass of adsorbent: 100 g. (**a**) Breakthrough curve; (**b**) temperature trend.
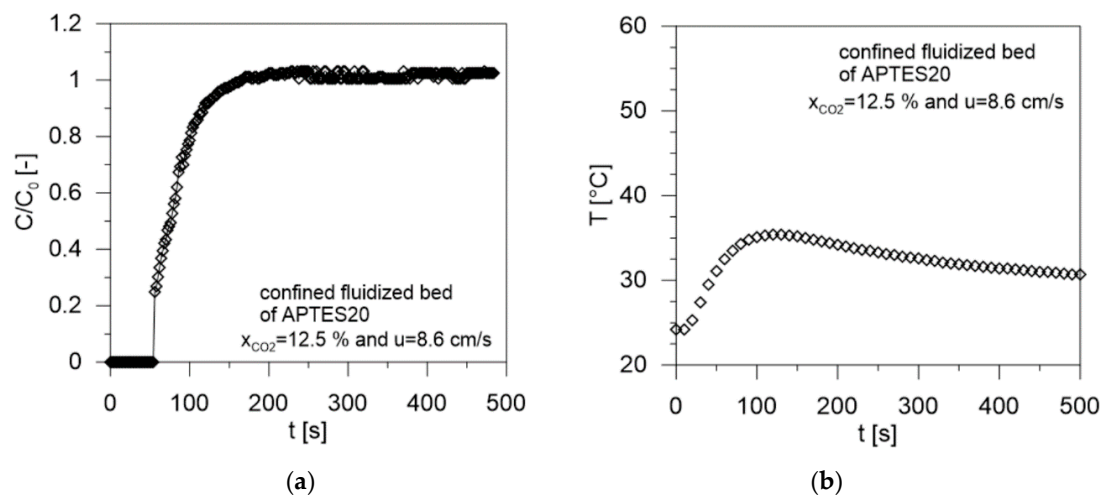
Figure 14. Adsorption test for APTES20 in a confined bed at u = 8.6 cm/s. Mass of adsorbent: 100 g. (**a**) Breakthrough curve; (**b**) temperature trend.
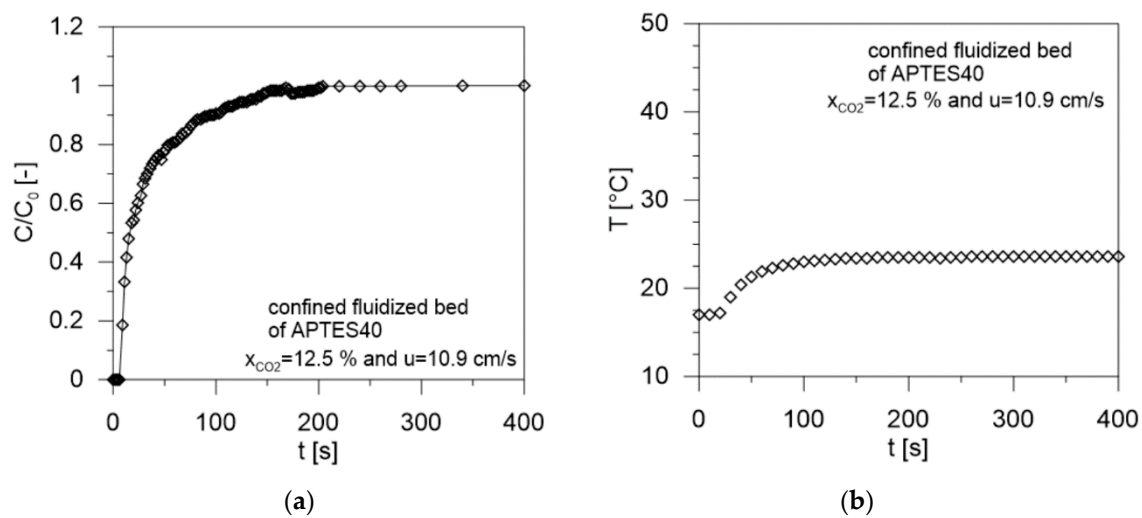
(a) (b)

Figure 15. Adsorption test for APTES40 in a confined bed at u = 10.9 cm/s. Mass of adsorbent: 100 g. (**a**) Breakthrough curve; (**b**) temperature trend.

The characteristic contact time for this continuous process is defined as

$$t_c = V_{open}/Q_{mix} \tag{3}$$

where

$$V_{open} = AH_{fc}\varepsilon_p - \frac{m}{\rho} \tag{4}$$

and the inlet flow rate of the gas mixture fed to the column is

$$Q_{mix} = Au = Q_{air} + Q_{CO2} \tag{5}$$

To determine the flow rates of both gases used in the experiments, the CO_2 fraction, x_{CO2}, and the gas velocity of the mixture, u, have to be set as an input for the following relationships:

$$Q_{CO2} = x_{CO2}Au \tag{6}$$

$$Q_{air} = (1 - x_{CO2})Au \tag{7}$$

From each breakthrough curve the main parameters were determined: the breakthrough time, the saturation time, the fraction of bed utilized at the breakpoint and the amount of CO_2 adsorbed.

The breakthrough time t_b, or breakpoint, is the time at which CO_2 at the outlet of the adsorption column reaches 5% of the inlet concentration. Usually, in a continuous process, it represents the time at which the gas feed must be switched to a stand-by column while the saturated sorbent of the first column is regenerated.

The saturation time, t_s, is the time at which CO_2 at the outlet of the adsorption column reaches 95% of the inlet concentration.

The fraction of bed utilized at the breakpoint, W, represents the ratio between the amount of CO_2 adsorbed up to the breakpoint and that adsorbed at saturation. This parameter is strictly related to the performance of the sorbent; for a given contact time, the higher W the lower the amount of sorbent required. Conversely, for a fixed mass of solid in the column, a higher value of W indicates that sorbent saturation occurs after a longer time.

Finally, the mass of CO_2 adsorbed per unit mass of adsorbent, m_{CO2} (reported as mg of CO_2 adsorbed per gram of sorbent) is calculated by integration of the breakthrough curve. This is the main parameter to analyze when different adsorbents are compared.

The maximum temperature T_{max} reached during the adsorption test (measured by the thermocouple immersed in the bed) allowed us to check also the thermal effects associated with the process. All the value of these parameters are shown in Table 4.

Table 4. Adsorption test data for both amino-functionalized samples at various fluidization velocities.

Sample	Gas Velocity u [cm/s]	Contact Time t_c [s]	Breakthrough Time t_b [s]	Saturation Time t_s [s]	CO$_2$ Adsorbed m_{CO2} (mg/g$_{solid}$)	W (g/g %)	T_{max} (°C)	CO$_2$/N Molar Ratio [-]	Efficiency (%)
As-made Silica	3.7	1.09	5	10	6.15	68.7	25.5		
APTES20	5.7	0.68	104	170	29.9	78.0	36.5	0.935	100
	8.6	0.57	54	128	29.6	65.0	35.4	0.926	
APTES40	6.9	0.64	11	219	32.5	20.5	27.7	0.665	82.8
	10.9	0.49	6	134	31.3	17.0	23.6	0.641	

Even if the gas velocities in the expansion regime are different, their values are comparable as they represent conditions in which the distance from the onset of fluidization is constant; in the first case the value of u is c.a. 25% higher than u_{mfc} of the solid, thus corresponding to a low level of expansion of the bed; in the second case, with a value of u c.a. 93% higher than u_{mfc}, the bed of sorbent reached an extended homogeneous expansion. This circumstance is confirmed by contact time values, reported in the Table 4, which are very close at similar expansion conditions.
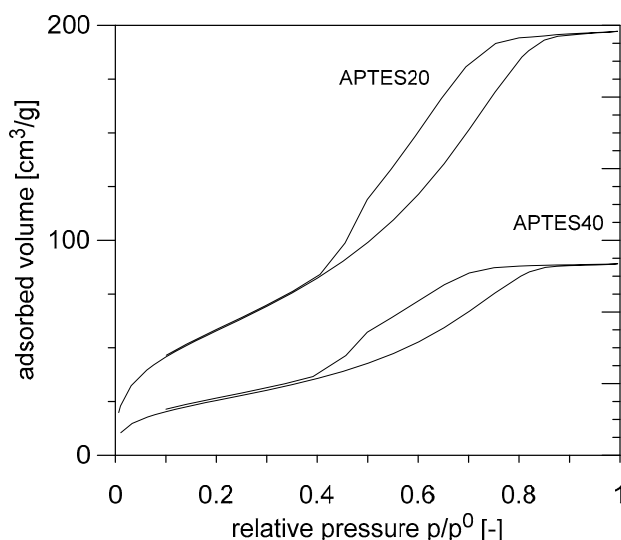
3.3. Thermal Stability

Usually, CO$_2$ adsorption involves a reaction between the acidic CO$_2$ molecules and the modified basic active sites and for this reason amine–based adsorbents are extensively studied with regard to enhancing CO$_2$ adsorption capacity and selectivity [7]. Amine impregnation is advantageous because it increases tolerance to water vapor in the gas feed of mesoporous silicas. On the other hand, several disadvantages are also present including high regeneration cost, equipment corrosion and oxidative degradation of some amines [21]. To investigate this last aspect, special attention has been devoted to the thermal stability of sorbents investigated here.

Figure 16 reports the TG thermograms of APTES20 (a) and APTES40 (b), respectively, after different cycles of regeneration. In the APTES20 sample, the initial amount of organic was ca. 16%, with a decrease to 14% after the first cycle of regeneration, a value that remains constant during all the other cycles of CO$_2$ adsorption. On the other hand, the APTES40 sample (24.56% total weight loss before the adsorption tests) shows a weight loss of ca. 24% after the first cycle of adsorption; such a value decreases to 20% and then remains constant after the ninth cycle.
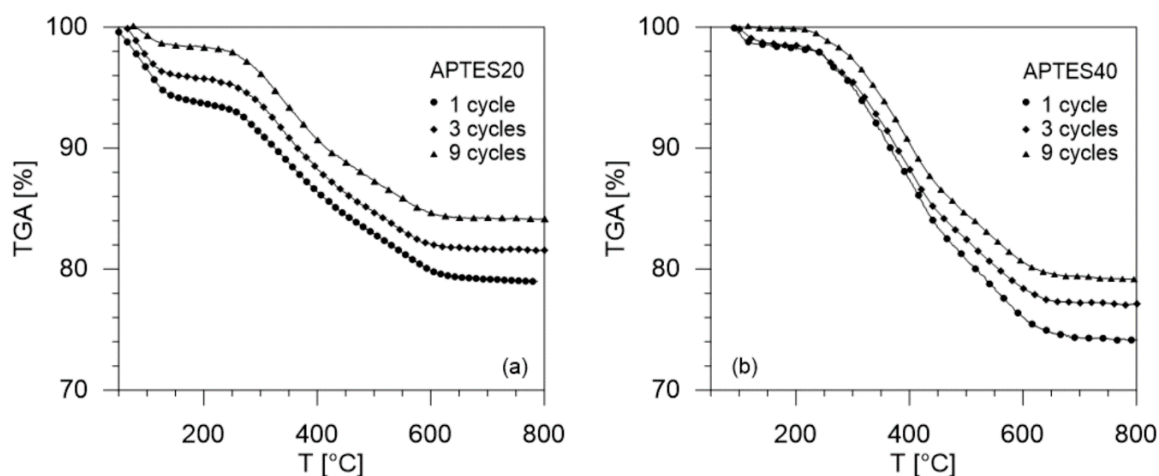
Figure 16. TG analysis for (**a**) APTES20 and (**b**) APTES40 after various cycles of adsorption/regeneration.

The nitrogen adsorption/desorption isotherms of APTES20 and APTES40 samples after nine cycles of regeneration, reported in Figure 17, support the results presented above. First of all, the shapes of the two isotherms are very similar to those obtained from the as-prepared samples (see Figure 5). On the other hand, S_{BET} and pore volume are slightly higher with respect to the values reported in Table 2. Specific surfaces are 226 and 98 m^2/g for APTES20 and APTES40, respectively. In the same way the pore volume increases to 0.30 and 0.14 g/cm^3. The combination of all these results allows us to affirm that during the exhaustion/regeneration cycles only the organic molecules weakly linked to the silica surface are removed. It is likely that the amount of easily desorbed molecules is lower in APTES20.

Figure 17. Nitrogen adsorption–desorption isotherms for the two amino-functionalized samples after ninth cycle of adsorption/regeneration.

These results are associated with high thermal stability and are in good agreement with those obtained by Quang et al. [19], indicating that the amino groups are linked to the silica surface by chemical bonds.

4. Discussion and Conclusions

From the analysis of Figures 12a, 13a, 14a and 15a and of data of Table 4, it can be noticed that the breakthrough curve for the sample APTES20 has a higher breakpoint time, indicating that this sorbent can capture CO$_2$ for a longer time during an industrial process; moreover, the saturation time is lower than that of the sample APTES40, suggesting that faster kinetics of adsorption are related to a larger availability of active surface.

The amount of CO$_2$ adsorbed, calculated by integration of the breakthrough curve, is slightly higher for APTES40. Nevertheless, this sample exhibits remarkably lower values of *W*, indicating a slow saturation kinetic and consequently an insufficient use of the sorbent up to the breakpoint. This behaviour is incompatible with industrial applications when switching to regeneration of the sorbent at the breakpoint is required. On the whole, the values of CO$_2$ adsorbed measured, over 30 mg/g, are better than the result obtained by Leal et al. [22], equal to 26.4 mg/g at 23 °C.

Regarding the effect of the operating gas velocity, its increase reduces the contact time but does not modify the process performance in terms of the mass of CO$_2$ adsorbed. In a previous work [14], it has been demonstrated that the increase in gas velocity can improve the control of the thermal effects of the adsorption process. As Figures 12b, 13b, 14b and 15b show, for the amino-functionalized silica used in this experimental investigation the thermal effects are moderate, resulting in a variation of 10 °C for APTES20 and of only 5 °C for APTES40. Though small in all cases, the increase in the adsorption

temperature depends on the operating gas velocity of the process (see T_{max} in Table 4); this is consistent with previous findings [14] indicating that lower temperatures are measured at higher gas velocities.

The experimental results of Quang et al. [19] have shown that the nitrogen content in the adsorbent increases with the increase in APTES concentration in the solid, but also that a maximum CO_2 load exists. At a high concentration, APTES soaked in the pores produces a pore blockage so that CO_2 gas cannot access hidden amine sites, a circumstance that causes a reduction in CO_2 adsorption. For this reason, in our study lower APTES concentrations have been explored, as the new gas–solid contact configuration provided by the packed-fluidized bed mass transfer is improved thanks to the extension of the expansion regime. In fact, APTES20 offered the best performance for a potential industrial application of CCS: high CO_2 capture ability, fast kinetics of adsorption, good efficiency of use of the sorbent in a continuous process, small thermal effects at long contact times and high stability for long-term operation with the optimum adsorption and regeneration temperature of 120 °C. Finally, APTES20 sample preparation consumes a lower amount of an expensive organic reactant.

In conclusion, as-made silica did not show any remarkable CO_2 adsorption capacity, consistently with what was expected. In any case, the material confirmed the role of heterogenous support able to allow an efficient dispersion of the adsorption sites. On the contrary, APTES-functionalized samples showed a significantly higher CO_2 adsorption capacity. Such a capacity is of the same order of magnitude for the two materials, although the process kinetics are different. When all the aspects of the process are considered, it can be concluded that APTES20 offers a better performance in a continuous process.

Author Contributions: Conceptualization, R.G. and F.T.; methodology, R.G.; software, M.G.; validation, R.G., F.T. and M.G.; formal analysis, R.G. and F.T.; investigation, R.B. and G.L.; resourses, R.G. and F.T; data curation, R.G. and F.T.; writing—original draft preparation, R.G.; writing—review and editing, R.G., F.T. and B.F.; visualization, R.G.; supervision, B.F.; project administration, F.T.; funding acquisition, F.T. and B.F. All authors have read and agreed to the published version of the manuscript.

Conflicts of Interest: The authors declare no conflict of interest.

Notation

A	column section, cm^2
C/C_0	dimensionless CO_2 fraction in the effluent gas, -
D	column diameter, cm
d_V	volume diameter of sorbent, μm
H_{fc}	sorbent height in confined bed, cm
m_{CO2}	mass of CO_2 adsorbed per unit mass of sorbent, mgCO_2/g sorbent,
m	mass of sorbent bed, g
n	expansion index, -
Q_{air}	volumetric flow rate of air, cm^3/s
Q_{CO2}	volumetric flow rate of gas mixture, cm^3/s
Q_{mix}	volumetric flow rate of gas mixture, cm^3/s
t	time, s
t_b	breakthrough time in the confined bed, s
t_c	contact time in the confined bed, s
t_s	saturation time in the confined bed, s
T	temperature in the middle of the confined fluidized bed, °C
T_{max}	maximum temperature in the middle of the confined fluidized bed, °C

u	superficial gas velocity, cm/s
u_{mfc}	minimum fluidization velocity of the confined bed, cm/s
u_0	maximum expansion velocity of the confined bed, cm/s
V	geometrical volume of the solid, cm^3
V_{open}	volume available to gas, cm^3
W	fraction of bed utilized at breakpoint, %
x_{CO2}	CO_2 fraction in the inlet gas, % vol

Greek Symbols

ΔP_{conf}	pressure drop in the confined system, Pa
ε	voidage in the packed-fluidized bed, -
ε_{fc}	voidage of the equivalent conventional bed, -
ε_p	voidage of the packed bed, -
ρ	particle density of solid, kg/m^3

References

1. Harvey, C.; Gronewold, N. CO_2 emissions will break another record in 2019. *E&E News*, 4 December 2019.
2. Wang, Y.; Zhao, L.; Otto, A.; Robinius, M.; Stolten, D. A Review of post-combustion CO_2 capture technologies from coal-fired power plants, energy. *Procedia* **2017**, *114*, 650–665.
3. Haszeldine, R.S. Carbon Capture and Storage: How Green Can Black Be? *Science* **2009**, *325*, 1647–1651. [CrossRef] [PubMed]
4. Rochelle, G.T. Amine Scrubbing for CO_2 Capture. *Science* **2009**, *325*, 1652–1654. [CrossRef] [PubMed]
5. Choi, S.; Drese, J.H.; Jones, C.W. Adsorbent Materials for Carbon Dioxide Capture from Large Anthropogenic Point Sources. *ChemSusChem* **2009**, *2*, 796–854. [CrossRef]
6. Sayari, A.; Belmabkhout, Y.; Serna-Guerrero, R. Flue Gas treatment via CO_2 adsorption. *Chem. Eng. J.* **2011**, *171*, 760–774. [CrossRef]
7. Yu, C.-H.; Huang, C.-H.; Tan, C.-S. A review of CO_2 capture by absorption and adsorption. *Aerosol Air Qual. Res.* **2012**, *12*, 745–769. [CrossRef]
8. Quang, D.V.; Rabindran, A.V.; El Hadri, N.; Abu-Zahra, M.R.M. Reduction in the regeneration energy of CO_2 capture process by impregnating amine solvent onto precipitated silica. *Eur. Sci. J.* **2013**, *9*, 82–102.
9. Wang, Z.L.; Ding, Y.L.; Ghadiri, M. Flow of a gas–solid two-phase mixture through a packed bed. *Chem. Eng. Sci.* **2004**, *59*, 3071–3079. [CrossRef]
10. Girimonte, R.; Vivacqua, V. The expansion process of particle beds fluidized in the voids of a packing of coarse spheres. *Powder Technol.* **2011**, *213*, 63–69. [CrossRef]
11. Girimonte, R.; Vivacqua, V. Design criteria for homogeneous fluidization of Geldart's class B solids upward through a packed bed. *Powder Technol.* **2013**, *249*, 316–322. [CrossRef]
12. Girimonte, R.; Vivacqua, V.; Formisani, B. Extension of the model of binary fluidization to beds confined in a packing of coarse spheres. *Powder Technol.* **2016**, *297*, 275–282. [CrossRef]
13. Girimonte, R.; Formisani, B.; Testa, F. Adsorption of CO_2 on a confined fluidized bed of pelletized 13X zeolite. *Powder Technol.* **2017**, *311*, 9–17. [CrossRef]
14. Girimonte, R.; Formisani, B.; Testa, F. CO_2 adsorption in a confined fluidized bed of zeolite pellets: Influence of operating velocity. *Particuology* **2019**, *46*, 67–74. [CrossRef]
15. Abrahamsen, A.R.; Geldart, D. Behaviour of gas-fluidized beds of fine powders, part I. Homogeneous expansion. *Powder Technol.* **1980**, *26*, 35–46. [CrossRef]
16. Brunauer, S.; Emmett, P.H.; Teller, E. Adsorption of gas in multimolecular layers. *J. Am. Chem. Soc.* **1938**, *60*, 309–319. [CrossRef]
17. Barrett, E.P.; Joyner, L.G.; Halenda, P.P. The Determination of Pore Volume and Area Distributions in Porous Substances. I. Computations from Nitrogen Isotherms. *J. Am. Chem. Soc.* **1951**, *73*, 373–380. [CrossRef]
18. Thommes, M.; Kaneko, K.; Neimark, A.V.; Olivier, J.P.; Rodriguez-Reinoso, F.; Rouquerol, J.; Sing, K.S.W. Physisorption of gases, with special reference to the evaluation of surface area and pore size distribution (IUPAC Technical Report). *Pure Appl. Chem.* **2015**, *87*, 1051–1069. [CrossRef]

19. Quang, D.V.; Hatton, T.A.; Abu-Zahra, M.R.M. Thermally stable amine-grafted adsorbent prepared by impregnating 3-Aminopropyltriethoxysilane on mesoporous silica for CO_2 capture. *Ind. Eng. Chem. Res.* **2016**, *55*, 7841–7852. [CrossRef]

20. Xu, X.; Song, C.; Andresen, J.M.; Miller, B.G.; Scaroni, A.W. Novel Polyethylenimine-Modified Mesoporous Molecular Sieve of MCM-41 Type as High-Capacity Adsorbent for CO_2 Capture. *Energy Fuels* **2002**, *16*, 1463–1469. [CrossRef]

21. Sayari, A.; Belmabkhout, Y. Stabilization of amine-containing CO_2 adsorbents: Dramatic effect of water vapour. *J. Am. Chem. Soc.* **2010**, *132*, 6312–6314. [CrossRef]

22. Leal, O.; Bolívar, C.; Ovalles, C.; García, J.J.; Espidel, Y. Reversible adsorption of carbon dioxide on amine surface-bonded silica. *Inorg. Chim. Acta* **1995**, *240*, 183–189. [CrossRef]

Publisher's Note: MDPI stays neutral with regard to jurisdictional claims in published maps and institutional affiliations.